Contents lists available at ScienceDirect

Anterior insular sortex is a bottleneck of sognitive sontrol

ingting Wu[a,1], Xingchao Wang[b,c,1], Qiong Wu[d,e,1], Alfredo Spagna[f,g], Jiaqi Yang[h], Changhe Yuan[i], Yanhong Wu[e,***], Zhixian ●ao[b,c,**], Patrick R. Hof[j,k], Jin Fan[a,j,k,l,*]

[a] Department of Psychology, Queens College, The City University of New York, Queens, NY, USA
[b] Department of Neurosurgery, Beijing Tiantan Hospital, Capital Medical University, Beijing, China
[c] China National Clinical Research Center for Neurological Diseases, Beijing, China
[d] School of Psychology, Capital Normal University, Beijing, China
[e] Beijing Key Laboratory of Behavior and Mental Health, School of Psychological and Cognitive Sciences, Peking University, Beijing, China
[f] Department of Psychology, Columbia University in the City of New York, USA
[g] Institut du Cerveau et de la Moelle épinière, ICM, INSERM U-1127, CNRS UMR 7225, Sorbonne Université, Paris, France
[h] Department of Computer Science, The Graduate Center, The City University of New York, New York, NY, USA
[i] Department of Computer Science, Queens College, The City University of New York, Queens, NY, USA
[j] Nash Family Department of Neuroscience, Icahn School of Medicine at Mount Sinai, New York, NY, USA
[k] Friedman Brain Institute, Icahn School of Medicine at Mount Sinai, New York, NY, USA
[l] Department of Psychiatry, Icahn School of Medicine at Mount Sinai, New York, NY, USA

AR ICLE INFO

Keywords:
Anterior cingulate cortex
Anterior insular cortex
Cognitive control
Cognitive control capacity
Cognitive control network

ABS RAC

Cognitive control, with a limited capacity, is a core process in human cognition for the coordination of thoughts and actions. Although the regions involved in cognitive control have been identified as the cognitive control network (CCN), it is still unclear whether a specific region of the CCN serves as a bottleneck limiting the capacity of cognitive control (CCC). Here, we used a perceptual decision-making task with conditions of high cognitive load to challenge the CCN and to assess the CCC in a functional magnetic resonance imaging study. We found that the activation of the right anterior insular cortex (AIC) of the CCN increased monotonically as a function of cognitive load, reached its plateau early, and showed a significant correlation to the CCC. In a subsequent study of patients with unilateral lesions of the AIC, we found that lesions of the AIC were associated with a significant impairment of the CCC. Simulated lesions of the AIC resulted in a reduction of the global efficiency of the CCN in a network analysis. hese findings suggest that the AIC, as a critical hub in the CCN, is a bottleneck of cognitive control.

1. Introduction

Cognitive control, which coordinates mental operations under conditions of uncertainty at perceptual or higher levels so that decisions can be made (Fan et al., 2014), is supported by the cognitive control network (CCN) in the brain (Fan et al., 2014; Niendam et al., 2012; Wu et al., 2018). he CCN is a large-scale network composed of two subnetworks: (1) the frontoparietal network (FPN), including the frontal eye field (FEF) and supplementary eye field, mid frontal gyrus (MF●), areas near and along the intraparietal sulcus (IPS) and superior parietal lobule (Corbetta, 1998; Fan et al., 2014); (2) the cingulo-opercular network (CON), including the anterior cingulate cortex (ACC) and anterior insular cortex (AIC) (Dosenbach et al., 2007, 2008); and (3) subcortical structures, including the thalamus and basal ganglia (Fan et al., 2014; Koziol, 2014; Rossi et al., 2009). It is known that the cognitive control system has a severely low upper limit (Posner and Snyder, 1975). According to information theory (Shannon and Weaver, 1949), this upper limit can be quantified as the capacity of an information processing channel, i.e., the maximal amount of information that can be processed during a certain period of time. Under an information theory framework of cognitive

* Corresponding author. Department of Psychology, Queens College, he City University of New York, 65-30 Kissena Blvd., Queens, NY, 11367, USA.
** Corresponding author. Department of Neurosurgery, Beijing iantan Hospital, Capital Medical University, No.6, ian an XiLi, Dongcheng District, Beijing, 100050, China.
*** Corresponding author. School of Psychological and Cognitive Sciences, Peking University, Wusi Road, Haidian, Beijing, 100871, China.
E-mail addresses: wuyh@pku.edu.cn (Y. Wu), zhixian_g@hotmail.com (Z. ●ao), jin.fan@qc.cuny.edu (J. Fan).

[1] Co-first authors.

https://doi.org/10.1016/j.neuroimage.2019.02.042
Received 28 October 2018; Received in revised form 1 February 2019; Accepted 17 February 2019
Available online 21 February 2019

control (Fan, 2014), we have recently quantified the capacity of cognitive control (CCC) as approximately 3–4 bits per second (bps) (Wu et al., 2016). However, the neural mechanisms limiting the CCC remain unclear.

A potential mechanism of this capacity limit could be the existence of a single bottleneck region or subnetwork of the CCN exerting a heavy working load due to its concurrent involvement in multiple processes during cognitive control (i.e., an integrative hub) (De Baar, 1994; orban et al., 2011; Watanabe and Funahashi, 2014). he AIC appears to be the best candidate as a bottleneck region that determines the CCC. It receives information from multiple modalities (e.g., visual, auditory, somatosensory, motor, and autonomic nervous systems) and domains (e.g., exteroception, interoception, emotion, and language) (Ackermann and Riecker, 2004; Augustine, 1996; Bamiou et al., 2003; Chang et al., 2012; Critchley et al., 2004), and re-represents the vast information to generate higher-level abstract and subjective information that are considered as “thoughts”, “feelings”, and “awareness” (Brass and Haggard, 2010; Craig, 2009, 2011; u et al., 2013; Nelson et al., 2010; Singer et al., 2009). he AIC has abundant anatomical connections with diverse parts of the brain (Augustine, 1996; Cauda et al., 2011, 2012; Cauda and Vercelli, 2012; Eckert et al., 2009; Flynn, 1999; Kelly et al., 2012; Spagna et al., 2018a) which may support dynamic coordination among information processes in different large-scale brain networks (Cocchi et al., 2013; Menon and Uddin, 2010; Sridharan et al., 2008). Each of the functions of the AIC (e.g., encoding, integrating, switching, and controlling) requires and competes for the limited neural resources of this region. Inefficient information processing capacity in such a brain hub should significantly impair global communication (Albert et al., 2000; Power et al., 2013), and consequently, damage of the AIC may significantly impact the CCC.

Here we employed a perceptual decision-making task, the backward masking majority function task (MF -M) (Wu et al., 2016), to challenge cognitive control by manipulating both information amount (measured as information entropy), which depends on both uncertainty of inputs at perceptual level and higher-level mental algorithms to make the decision, and the exposure time (E) of the stimuli so that the amount of to-be-controlled information during a unit of time (i.e., information rate, referred as cognitive load in this study) could be varied within a wide range, and therefore the CCC of each participant could be estimated based on the relationship between cognitive load and response accuracy. We tested the role of the AIC as a bottleneck of cognitive control by examining (1) the relationship between its activity and cognitive load as well as the relationship between its activity and CCC in a functional magnetic resonance imaging (fMRI) study, and (2) the necessity of the AIC in supporting the CCC in a human lesion study. he mechanism of the AIC, in comparison to the ACC, in relation to the CCC was further explored by combining complex network analyses with lesion simulations.

2. Materials and methods

2.1. Participants

Adults with no history of head injury, psychiatric, and neurological disorders ($n = 32$) participated in the fMRI study. All participants were right-handed and had normal or corrected-to-normal vision. We excluded one participant for poor image quality and an additional four participants because of high percentage (>5%) of missing responses. he final sample size was 27 (15 females and 12 males; mean ± standard deviation [SD] age, 25.6 ± 4.6 years). he Institutional Review Boards (IRB) of he City University of New York (CUNY) and of the Icahn School of Medicine at Mount Sinai (ISMMS) approved the protocol and written informed consent was obtained from each participant before participation.

In the lesion study, we recruited patients with a focal lesion of the AIC (AIC group, $n = 8$), patients with a focal lesion of the ACC (ACC group, $n = 7$), and patients with a focal lesion outside the CCN regions as brain damage controls (BDC group, $n = 9$, eight with a lesion in the temporal pole, and one with a lesion in the frontal pole) from the Patient's Registry of iantan Hospital, Beijing, China. All lesions were unilateral. We also recruited participants with no history of head injury, psychiatric, and neurological disorders as neurologically intact controls (NIC group, $n = 27$) from local Beijing communities. All participants were right-handed and had normal or corrected-to-normal vision. he demographic information (including gender, age, and education) was matched across groups. All participants completed the Mini-Mental State Examination (MMSE) (Cockrell and Folstein, 1988) and the Beck Depression Inventory (BDI) (Schwab et al., 1967) questionnaires for assessment of cognitive ability and mood state, respectively (see Supplementary Materials and Supplementary able 1 for details). One patient in the ACC group and one patient in the BDC group were excluded from further analyses because they did not follow the instruction to make a response in at least 95% of the trials. he IRB of iantan Hospital of the Capital Medical University in Beijing approved the protocol and written informed consent was obtained from each participant.

Table 1
Estimates of information amount and information rate in each task condition, and the contrast vector of each effect.

	Congruency	E (ms)			
		250	500	1000	2000
Estimates					
Information entropy (bit)	5:0	1.58	1.58	1.58	1.58
	4:1	2.91	2.91	2.91	2.91
	3:2	4.91	4.91	4.91	4.91
1/E (1/s)	5:0	4	2	1	0.5
	4:1	4	2	1	0.5
	3:2	4	2	1	0.5
Information rate (bps)	5:0	6.32	3.16	1.58	0.79
	4:1	11.64	5.82	2.91	1.46
	3:2	19.64	9.82	4.91	2.46
Contrast vectors					
Information entropy	5:0	−0.87	−0.87	−0.87	−0.87
	4:1	−0.13	−0.13	−0.13	−0.13
	3:2	1.00	1.00	1.00	1.00
1/E	5:0	1	0.06	−0.41	−0.65
	4:1	1	0.06	−0.41	−0.65
	3:2	1	0.06	−0.41	−0.65
Interaction	5:0	−0.87	−0.05	0.36	0.57
	4:1	−0.13	−0.01	0.05	0.08
	3:2	1	0.06	−0.41	−0.65

Note: E refers to exposure time. Information entropy is a measure of information amount in each congruency condition. Information rate is a measure of

2.2. The backward masking majority function task

o make a decision under conditions of uncertainty at either perceptual or higher levels, cognitive control is employed to coordinate mental operations. he majority function task (MF) requires participants to indicate the direction majority of a set of left and right-pointing arrows displayed on the screen (e.g., with 2 left-pointing arrows and 3 right-pointing arrows). In our previous studies using the MF , we have demonstrated that a sophisticated algorithm that consists of a series of binary decision-making processes has to be adopted to reach the final decision of the majority (Fan et al., 2008; Wang et al., 2011). he information amount, determined by both inputs (the ratio of left- and right-pointing arrows and the set size) and mental algorithms, estimated under the framework of information theory as information entropy in unit of bit, varied from 0 to 4.91 bits. his range is much wider than in the flanker task (Eriksen and Eriksen, 1974) and the color-word Stroop task (Stroop, 1935), which are classical cognitive control tasks that only require a single binary decision-making process with information entropy ranging from 0 to less than or equal to 1 bit (Fan, 2014; Mackie et al., 2013). herefore, cognitive control is more challenged by the MF compared to these tasks.

According to information theory (Shannon and Weaver, 1949), when the amount of information to-be-processed during a unit of time (information rate in bps) exceeds a channel's capacity, the communication accuracy starts to decline and eventually reaches the chance level when the information rate is too high. In the MF , the E of the arrow sets was fixed to 2500 ms, and a relative high accuracy (about 75%, much higher than chance level of 50%) was observed under the condition with the highest cognitive load (Fan et al., 2008; Mackie et al., 2013), indicating that the cognitive load in this task was not high enough to challenge the CCC. o further challenge cognitive control, we additionally manipulated the E using a backward masking approach (i.e., following the presentation of a target set for a duration of time, which is the E , a mask set was displayed to prevent further visual processing of the target) so that right), 4:1 (4 left with 1 right or 4 right with 1 left), or 3:2 (3 left with 2 right or 3 right with 2 left). he E could be 250, 500, 1000, or 2000 ms. able 1 provides the estimates of information amount (measured as information entropy), the reciprocal of E (i.e., 1/E), and cognitive load (measured as information rate, which can be computed as entropy/E) in each task condition. Fig. 1b and c show the information entropy in each congruency condition and the information rate in each task condition, respectively. he information rate increases as a function of both information entropy and the reciprocal of E with a superadditive effect. In the fMRI study, there were 12 null trials as a 5000-ms fixation period, in addition to 36 test trials in each run. he congruency was varied within each run with 12 trials under each congruency condition. he E was varied between runs with three runs for each E , and there were 12 runs in total. For each participant, the presentation of the trials within each run was in a random order across all levels of congruency, and the presentation of runs was also in a random order across all E s. he exposure time was manipulated between blocks to avoid speed-accuracy trade-off, and the congruency was manipulated within block to keep participants' attention on the task. At the beginning and end of each run, there was a 30 s fixation period in the fMRI study and a 3 s fixation period in the lesion study. In the fMRI study, each run was composed by 48 trials (36 task trials and 12 null trials) and lasted 300 s. In total, 432 task trials were presented, and the task took approximately 68 min to be completed. In the lesion study, each run was composed by 36 task trials without any null trial and lasted 213 s. In total, there were 432 task trials presented and the task took approximately 43 min. Additional information about the testing procedure can be found in the Supplementary Materials.

2.3. Estimation of the capacity of cognitive control

For each participant, response accuracy was used to estimate the CCC (Wu et al., 2016). According to the definition of the capacity of a channel (Shannon and Weaver, 1949), we assumed that the probability of obtaining a correct response (equivalent to response accuracy) was determined by the difference between the amount of to-be-processed information and the amount that can be processed, i.e., the CCC. When the cognitive load is increased but is still lower than the CCC, the responses should be accurate. However, when the cognitive load exceeds the CCC, there should be a drop in response accuracy. he cognitive load was calculated using the congruency and E in a grouping search model demonstrated in our previous studies (Fan et al., 2008; Wang et al., 2011; Wu et al., 2016). In this model, participants keep randomly drawing a subset of stimuli from the given stimuli set, with the sample size as the majority size (N_{maj}, which is 3 for the set size of 5), until a congruent sample (i.e., all arrows pointing to the same direction) is obtained. he arrow direction in this congruent sample is then returned as the final response. he estimated amount of to-be-processed information (information entropy) can be estimated as the $\log_2$ transformation of the averaged number of to-be-processed arrows to reach a congruent sample. Each participant's CCC limits the amount of can-be-processed information under each E . A correct response would be made if a congruent sample can be obtained within the E , otherwise a random guessing response would be made. herefore, the expected response accuracy (E [accuracy]) is as:

$$E[accurac\ ] = P_{congruent} \times p_0 + \left(1 - P_{congruent}\right) \times p_{guess},$$

in which p_0 is the baseline response accuracy when a congruent sample is obtained, p_{guess} is the chance level of accuracy for guessing (50%), and $P_{congruent}$ is the probability that at least one congruent sample can be obtained within a given E . he $P_{congruent}$ can be calculated as 100% minus the probability of obtaining no congruent sample within the E , which is $P_{miss}{}^{n_s}$, with P_{miss} as the probability of obtaining an incongruent sample by one attempt of search and n_s as the number of attempts. he P_{miss} is determined by the congruency of an arrow set (see Supplementary Materials for details), while n_s is determined by the amount of information that can be processed within a unit of time (parameter C), N_{maj}, and E , expressed as $n_s = 2^C \times ET/N_{maj}$. he final equation is

$$E[accurac\ ] = \left[1 - P_{miss}^{\frac{2^C \times ET}{N_{maj}}}\right] \times p_0 + P_{miss}^{\frac{2^C \times ET}{N_{maj}}} \times p_{guess}.$$

he estimated CCC is the value of C that provides the best global fitting of the predicted response accuracy to the empirical response of each participant across all conditions. A high CCC indicates that more information can be accurately processed during a given period, leading to high response accuracy in task conditions with high information rate (as the index of cognitive load). See Supplementary Materials for details of the estimation of the CCC, as well as the computation of the mean response accuracy and reaction time (R) in each condition. he R was not included in the model for the estimation of the CCC. In our previous study for the task development and CCC estimation (Wu et al., 2016), we found that although there was a weak improvement in model fitting by including R compared to the model used in the current study without including R , the reliability of the estimation was impaired.

2.4. Intelligence quotient (IQ) measurement

For the fMRI study, the IQ of each participant was measured using a short form of the Wechsler Adult Intelligence Scale – Fourth Edition (WAIS-IV), which included three subtests: Symbol Search, Vocabulary, and Figure Weight. his combination is one of the best three-subtest short-form combinations, with high reliability (.935) and validity (.915) coefficients (Sattler and Ryan, 2009). he raw score of each subtest was converted to the scaled score for the individual's age group. he total scaled score across the three subtests was then converted to the estimated FSIQ following the ellegen and Briggs (1967) procedure.

2.5. fMRI data acquisition

MRI acquisitions were obtained at ISMMS on a 3 Siemens Magnetom Skyra scanner with a 16-channel phase-array coil. Each scan session lasted about 1.5 hour. All images were acquired along axial planes parallel to the anterior commissure-posterior commissure (AC-PC) plane. welve runs of 2*-weighted images for fMRI were acquired with a gradient-echo planar imaging (●E-EPI) sequence with the following parameters: 40 axial slices of 4 mm thick, interleaved, skip = 0 mm, R = 2000 ms, E = 27 ms, flip angle = 77°, FOV = 240 mm, matrix size = 64 × 64, voxel size = 3.8 × 3.8 × 4 mm. Each run began with two dummy volumes before the onset of the task to allow for equilibration of 1 saturation effects, followed by the acquisition of 150 volumes. A high-resolution 1-weighted anatomical volume of the whole brain was also acquired with a magnetization-prepared rapid gradient-echo (MPRA●E) sequence with the following parameters: 176 axial slices of 0.9 mm thick, skip = 0 mm, R = 2200 ms, E = 2.51 ms, flip angle = 8°, FOV = 240 mm, matrix size = 256 × 256, voxel size = 0.9 × 0.9 × 0.9 mm.

2.6. fMRI data analysis

2.6.1. Image preprocessing

Event-related fMRI data analysis was conducted using the Statistical Parametric Mapping package (SPM 12, RRID: SCR_007037; Welcome rust Centre for Neuroimaging, London, UK). he 1 image and all EPI images were manually adjusted to align the AC-PC plane. For each participant, each EPI image volume was realigned to the first volume and then slice timing corrected using the first slice as the reference. he 1 image was then coregistered to the mean EPI image using normalized mutual information. he coregistered 1 image was segmented into grey matter, white matter, cerebrospinal fluid, bone, soft tissue, and air/

background according to the SPM tissue probability map (Mazziotta et al., 1995), with affine regularization as ICBM space template – European brains. Realigned EPI images were then spatially normalized using the forward deformation field estimated in segmentation, resampled to a voxel size of $2 \times 2 \times 2$ mm. Normalized EPI images were then spatially smoothed with a ●aussian kernel of 8 mm full-width half-maximum.

2.6.2. General linear modeling

If a brain region is associated with the CCC, it should show the following two properties. First, the activation of this region should match the pattern of information rate (Fig. 1c). his property was examined by the conjunction of a main effect of information entropy, a main effect of the reciprocal of E , and the superadditive interaction effect. Second, this superadditive activation should be positively correlated to the CCC across participants, because a greater superadditive interaction effect in activation of this region indicates a better response to the demand of an increase in information rate, which determines the CCC.

First-level (single-subject level) statistical analyses of the event-related BOLD signal of each participant were conducted to identify the significant relationship between the hemodynamic responses in brain regions and task events (Friston et al., 1994). For each run, three regressors were constructed based on the onset vectors of arrow sets corresponding to the three congruency conditions under each E in trials with correct responses. An additional nuisance regressor was constructed for each condition based on the onset vectors of the arrow set for trial(s) with incorrect responses in this condition if there were any (minimum 0 and maximum 3 nuisance regressors in each run). he duration of these vectors were set as the E in the corresponding condition for the regressors mentioned above. o model out the feedback-related responses, two additional regressors were constructed for each run based on the onset vectors of feedback, with one for positive feedbacks and the other one for negative feedbacks. he durations of these vectors of feedbacks were set as 0. All of the above mentioned vectors were convolved with a standard hemodynamic response function (HRF) (Friston et al., 1998). he six motion parameters generated during realignment and sessions were entered into the model as additional nuisance covariates for each run. A high-pass filter with a 128-s cutoff was used to remove low-frequency signal drift, and serial correlation was estimated using an autoregressive AR (1) model (also for the following first-level ●LM analyses). he ●LM was estimated and the image of parameter estimate (β) for each regressor was obtained. For the arrow set-related regressors, the brain response to an event was modeled as the convolution of a standard HRF and a rectangular function with the E as the duration. he parameter estimate of each regressor (i.e., the β value) represents the change of HRF amplitude, while the convoluted hemodynamic response curve represents the cumulated BOLD responses across the duration. he area under a response curve depends on two factors: HRF amplitude and duration (E). By manipulating the information entropy and E , we can disassociate the contributions of information rate and processing time to BOLD responses. he estimated HRF amplitude is the brain response as a function of information rate. For a given value of information entropy, a large change in HRF amplitude could be associated with a high information rate due to a short E .

For the first-level analysis, a contrast image of all conditions versus baseline was generated by averaging the β values across the regressors for trials with correct responses. he linear main effect of information entropy was examined using the orthogonal polynomial contrast of entropy for 5:0, 4:1, and 3:2 congruency conditions, regardless of the E , based on the information entropy estimation of each congruency condition, and this contrast vector was demeaned to remove the zero-order term and by normalizing to an absolute maximum value. he linear main effect of the reciprocal of E was examined using the contrast based on the demeaned and normalized reciprocal of E regardless of congruency. he information entropy $\times$ reciprocal of E interaction was examined using the contrast as the scalar product between the contrast vectors of information entropy and the reciprocal of E . he positive interaction effect indicates a superadditive effect between the entropy and reciprocal of E , with stronger activation increase as entropy increases under conditions with shorter E than under conditions with longer E . It is worth noting that this interaction effect is statistically independent to the information rate because both entropy and the reciprocal of E were demeaned when computing the interaction. Contrast vectors are summarized in able 1.

Second-level group analyses were conducted to identify regions with significant activation changes across participants associated with each effect, including single condition versus baseline, all condition versus baseline (All-minus-Baseline), the main effects of information entropy and reciprocal of E , and the information entropy $\times$ reciprocal of E interaction. For each effect, the corresponding contrast image for each participant was entered in a random-effects statistical model that accounts for inter-subject variability and permits population-based inferences. One-sample t-tests were performed for each voxel. he conjunction analysis of the two main effects and their interaction was conducted. A positive effect in this conjunction indicates that the pattern of brain activation across task conditions matches the information rate as a function of information entropy, the reciprocal of E , and their interaction. A significance level for the height of each voxel of $p < .001$ (uncorrected) was used, together with a contiguous-voxel extent threshold (estimated based on the random field theory) to correct for multiple voxel comparisons resulting in cluster-level $p < .05$. his thresholding approach was also applied for the whole brain analyses described below.

A whole-brain voxel-wise second-level regression analysis was conducted to identify the superadditive activation regions that predict the CCC across participants. Contrast images of the information entropy $\times$ reciprocal of E interaction effect were entered in a random-effects model, with the CCC values of participants as the regressor, to conduct a voxel-wise regression analysis between the superadditive activation and the CCC.

2.6.3. Examination of the relationship between the neural involvement and cognitive load

o illustrate the regional activation in each task condition, we conducted regions of interest (ROI) analyses for regions that revealed a positive effect in the conjunction analysis. heir coordinates were defined as the corresponding positive local peaks in the second-level interaction contrast image (left AIC: [-32, 22, 0], right AIC: [32, 26, −8], left ACC: [-2, 18, 50], right ACC: [8, 28, 38]), which is statistically independent of the models in following ROI analysis. For each ROI, the first eigenvariate of the β value was extracted across all voxels within a sphere with 6 mm radius around the peak from the first-level single-condition-versus-baseline contrast map of each condition of each participant. he hemodynamic response curve within a 12 scans (24 s) window after the onset of arrows was reconstructed for each of these ROI using the MarsBaR toolbox (RRID: SCR_009605) (Brett et al., 2002).

Based on our previous studies (Wu et al., 2016), the activity of an information processing entity increases as a function of the rate of information input, and this increase is approximately linear when the information rate is lower than the capacity. he increase would start to slow down when the information rate exceeds the capacity until an activity plateau is reached (Buschman et al., 2011; Moreno-Bote et al., 2014). o test this pattern in the ROIs defined above, we adopted a non-linear capacity-limited model to fit the relationship between the regional activation (Y) of each ROI and cognitive load (i.e., information rate, I) as a logistic function: $Y = Y_0 + S * (1 - e^{-K * I})$, which is a typical function to describe a growth with plateau. Here Y_0 denotes the baseline activation when I is 0 bps, S denotes the span of the activity change when I rises from 0 to infinite, and K is the rate constant. he half-time of activity increase can be calculated as ln (2)/K, and the plateau of activity increase can be calculated as $S + Y_0$. his model was compared to a simpler linear function: $Y = Y_0' + K' * I$, where Y_0' denotes the baseline activation and K' denotes the rate of information processing, which indicates that no activation plateau is shown within the range of infor-

A mixed effect model with Y_0, S, and K as both fixed and random effects, and participant as the random effect was adopted to estimate parameters for each model, in which the restricted likelihood of the linear mixed-effect model (RELME) was used. he Bayesian information criterion (BIC) of each fitted mixed effect model, which takes likelihood, sample size, and number of free parameters into account, was used for the group-level model selection. For model comparison ($\Delta BIC = BIC_{linear} - BIC_{logistic}$), a $\Delta BIC > 2$ indicates positive evidence against the model with higher BIC ($\Delta BIC = 2$–6: positive; 6–10: strong; >10: very strong). he estimated model parameters and other statistics of model fitting (e.g., log likelihood, Akaike information criterion, and root mean squared residual) were also computed.

For the regions with the logistic function as the optimal model (i.e., left and right AIC), we compared the estimated parameters (i.e., Y_0, S, and half-time) between these two regions, using one-tailed pair-wise t-tests. Each index was calculated as the sum between the estimated fixed effect as a constant across participants and the random effect varying across participants. o examine how the activation changes in the right AIC determine the CCC, a Pearson correlation analysis was conducted between the CCC and each index (i.e., Y_0, S, and half-time).

2.6.4. Examination of the mediative role of AIC activation for the relationship between CCC and IQ

he relationship among the superadditive activation in the right AIC, CCC, and IQ was examined using mediation analyses (Baron and Kenny, 1986), with the CCC as the predictor (X), superadditive activation in the right AIC as the mediator (M), and IQ as the target variable (Y). We first examined the predictive effect of X to Y (path c: $Y = b_{10} + b_{11} \cdot X$) and the predictive effect of X to M (path a: $M = b_{20} + b_{21} \cdot X$). hen a regression model with both X and M as predictors ($Y = b_{30} + b_{31} \cdot X + b_{32} \cdot M$) was estimated if both paths a and c were significant. If the b_{32} (path b) is significant and b_{31} is smaller than b_{11}, M is a mediator between X and Y, with a non-significant b_{31} indicating a full mediation effect and a significant b_{31} indicating a partial mediation effect. his analysis was conducted for the FSIQ and each subscale of the IQ (i.e., Symbol Search subindex, Vocabulary subindex, scaled Vocabulary subindex, and Figure Weight subindex).

2.7. Comparison of the CCC across groups in the lesion study

2.7.1. Justification of the inclusion of groups

he design of the lesion study followed the logic used in our previous study (●u et al., 2012). o examine whether a lesion in the AIC, but not in the ACC, would lead to an impaired CCC, we included patients with a unilateral focal lesion of the AIC (the AIC group) and patients with a unilateral focal lesion in the ACC (the ACC group). he ACC group also served as an active control group to test whether a lesion in the other region of the CON would lead to a reduced CCC. We included a matched sample of neurologically intact controls (the NIC group) as a baseline reference of normal CCC. An additional group of patients with a lesion outside the CCN regions (brain damage controls, the BDC group) was recruited to exclude the potential explanation that the impaired CCC is due to brain surgical procedures *per se*, rather than the AIC or ACC lesion.

2.7.2. Lesion mapping

For each patient, brain regions with lesion were identified and plotted onto an anatomical template of a normal control (ch2. nii, provided by MRIcron: RRID: SCR_002403, http://www.cabiatl.com/mricro/mricro/index.html) by a neurosurgeon (X. W.). A group overlap of multiple lesions was created for each group using the MRIcron, with all lesions mapped on the right hemisphere.

2.7.3. Comparison of the CCC among groups

he estimated CCC values were compared among groups. If a region is necessary for cognitive control, the CCC in patients with lesions in this region should be significantly lower than in both NIC and BDC groups. In addition, the BDC patients should not be significantly different from the NIC participants to demonstrate that the impaired CCC is not due to the surgery procedure *per se*. he AIC and ACC groups were compared to the NIC and BDC groups as planned comparisons with Bonferroni correction applied.

For each comparison, the non-parametric bootstrapping method (Hasson et al., 2003; Mooney and Duval, 1993) was used to assess the probability of observing a between-group difference, because the current data set with a small sample size in each lesion group did not meet the assumptions of parametric statistics. his procedure was conducted with 10,000 iterations for each effect (e.g., the comparison between 8 AIC patients and 27 NIC participants). In each iteration: (i) a whole sample with all of the 35 participants from both AIC and NIC groups was created; (ii) 27 participants were randomly selected from the whole sample as the surrogate NIC sample; (iii) 8 participants were selected randomly from the whole sample as the surrogate AIC group; and (iv) the t-value (one-tailed, AIC < NIC) of the difference between the two surrogate groups was calculated. After the 10,000 iterations, the distribution of the t-values was obtained. he observed t-value of the CCC difference between the original AIC and NIC groups was calculated and compared along this t distribution. If the probability of obtaining the observed t-value along the permutated distribution of t-values was less than 5% (one-tailed), we considered the difference between the patient and control groups as significant.

2.8. Network analyses of the CCN

2.8.1. Single-trial brain response extraction

o estimate the task-evoked brain connectivity, we first extracted whole-brain single-trial responses using an "extract-one-trial-out" approach, as utilized in previous studies (Choi et al., 2012; Kinnison et al., 2012; Rissman et al., 2004; Wu et al., 2018). he single-trial responses (in β values) represent the change of brain activation associated with a specific event. Specifically, for each participant, a first-level ●LM was constructed for each trial, which included (1) all regressors of the first-level ●LM described in the above "●eneral linear modeling" section for the onsets of all corresponding events for each regressor convoluted with the HRF, as well as the nuisance regressors, with the onset of the event of the trial to be modeled excluded in its corresponding regressor, and (2) the regressor for this single trial to be modeled, which is the convolution of its onset vector with the HRF. he estimation of the ●LM was looped trial-by-trial across all trials. he single-trial brain response is the estimated β image of the single trial modeled. he detection and estimation power of this single-trial extraction approach has been demonstrated in our previous study (Wu et al., 2018).

2.8.2. Bayesian network construction

ROI-based Bayesian network analyses (Wu et al., 2018) were conducted to investigate the effective connectivity between regions of the CCN, and between the CCN and sensory regions (i.e., visual areas) for the event-related single-trial responses. Here the estimated effective connectivity can be considered as the dependence of response changes (the single-trial β values) across trials between ROIs, which reflects the modulation effects of the task conditions on the intrinsic connectivity driven by task-irrelevant BOLD signal fluctuation across time. Although the network structure can also be discovered by the stochastic Dynamic Causal Modeling (DCM) (Friston et al., 2011), which is a more classical approach to estimate the effective connectivity, the set size of our ROIs ($n = 14$, see below) is too large to be handled by DCM. Compared to the DCM, the Bayesian network analysis has advantage of computational efficiency.

he nodes of the networks were defined based on the conjunction of the main effect of information entropy and the main effect of the reciprocal of E , as clusters that passed the threshold of cluster-level $p < .05$ for this conjunction (i.e., the height threshold $p < .001$ with the extent threshold $k > 185$, estimated based on the random field theory). Fourteen nodes were included: four CON regions (left and right AIC, left and right ACC), four FPN regions (left and right FEF, left and right IPS), four subcortical regions (left and right thalamus, left and right caudate nucleus), and left and right visual areas. For each node, the first eigenvariate β value was extracted across all voxels in the corresponding cluster of each single-trial β image. hen for each node, its trial-by-trial first eigenvariate β values were extracted for each participant with all task trials included.

At first-level (single-subject level), the connectivity between nodes was estimated using the max-min hill-climbing (MMHC) Bayesian structure learning algorithm (samardinos et al., 2006). In this algorithm, the skeleton of the network (i.e., an undirected network consisting of the connections between nodes without their directions) is first learned by the Max-Min Parents & Children (MMPC) algorithm. After the MMPC procedure, the direction of each connection in the skeleton is estimated using the hill-climbing (HC) algorithm, which is a local search method. A bootstrapping strategy was used to identify the global fitting structure (Friedman et al., 1999), in which we generated 200 random datasets with each dataset containing 432 trials randomly sampled from the original task trials with replacement, and then one MMHC learned network was constructed for each random dataset. he bnlearn package (http://www.bnlearn.com) (Schwarz, 1978; Scutari and Nagarajan, 2011) was used to implement the MMHC algorithm. he outputs of the MMHC include the estimated strength and direction of each connection. For a connection between nodes i and j, the strength value is the frequency of the bootstrapped samples showing this connection, while the direction value is the probability of the connection from i to j. Both strength and direction values range from 0 to 1. For a pair of forward and backward connections between i and j (i.e., from i to j vs. from j to i), the strength values are identical, and the sum of the direction values is 1 if the strength value is greater than 0. he direction value is 0 if the strength value is 0. A 14×14 weighted directed connectivity matrix was constructed, with the connectivity value $(i, j; i \neq j)$ as the product of the strength value and the direction value. he values on the diagonal of this matrix were set as 0 as required by the complex network analyses.

After constructing the networks for each participant, we examined the significance of the network connections at group level. A pairwise t-test (two-tailed) was conducted between the empirical connectivity and the baseline connectivity for each connection across participants with a significance level of $p < .001$ (uncorrected) was adopted. Here the baseline connectivity was estimated by 1000 permutations for each participant. In each permutation, the values within each ROI were shuffled so that the correlation between each pair of nodes would be random. hen the corresponding connectivity matrix was constructed using the same Bayesian network construction procedure described above. he 1000 connection matrixes were averaged as the baseline connection matrix for each participant.

2.8.3. Graph analysis

o characterize the structure of the learned Bayesian networks, we conducted complex network analysis that measures topological properties of the networks using the Brain Connectivity oolbox (RRID: SCR_004841; brain-connectivity-toolbox.net) (Rubinov and Sporns, 2010). he community structure of the network was constructed by subdividing it into non-overlapping groups of nodes in a data-driven manner, i.e., by maximizing the possible numbers of within-group connections and minimizing the number of between-group connections. his estimated community structure was applied to all participants in the following estimations of the functional segregation and integration assuming that the brain networks of all participants share a common community structure.

For each participant, we examined whether the right AIC played a more important role as a connector hub for intermodular connections compared to the ACC in the estimated network by comparing their participation coefficient, which is a measurement of the centrality of nodes that quantifies the diversity of intermodular interconnections of each node. A node with a 0% participation coefficient indicates that it connects only with regions in its own module, while a participation coefficient of 100% indicates that it evenly connects with regions in all modules. A higher value indicates the greater importance of a node in facilitating global intermodular integration. Compared to the degree-based measures of centrality (i.e., the strength and betweenness centrality), the measure of the participation coefficient is more appropriate in identifying the hubs of brain networks that are critical to the communication among multiple systems (subnetworks) (Power et al., 2013). he participation coefficients for the inward connections (i.e., connections from other nodes to a given node) and the outward connections (i.e., connections from a given node to other nodes) were measured respectively. Pairwise t-tests (one-tailed) were conducted to test whether the participation coefficient of the right AIC was significantly higher than the participation coefficients of other regions, i.e., left AIC, left ACC, and right ACC. For the outward connections, because the left ACC had the highest participation coefficient across regions of the CON, we compared its participation coefficient to other regions in the CON using pairwise t-tests .1(of)-410.2(cen-)] Jrmr5.7(tBonferron)-688.7(orrec

Aectivity catrix tho-655.4(a)voi

declined as a function of both information entropy and the reciprocal of E until reaching chance level (Fig. 2a and Supplementary able 2; see Supplementary Materials for statistic details). hese results indicate that the input information could be processed accurately in conditions with low information rate, but the information processing became less accurate when the information rate was increased. For each participant, the CCC was estimated based on the response accuracy, and the group mean $\pm$ standard deviation (SD) of the CCC was 4.08 ± 0.67 bps (range: 2.81 to 5.38 bps; Supplementary Fig. 1). In addition, an increase in R was associated with an increase of both information entropy and E , indicating that the R increase as a monotonic function of the information entropy was constrained by E (Fig. 2

in the left and right ACC, with no significant negative effect found (Fig. 3d and able 2). Fig. 4a shows the pattern of the superadditive effect in terms of estimated HRF amplitude change in these regions. It is worth noting that while both R and HRF amplitude increased as a function of information entropy, there was a dissociation of the impact of E on R and on HRF amplitude: the R increased but the HRF amplitude decreased as a function of E . Supplementary Fig. 2 shows the cumulative hemodynamic responses (not HRF) in each task condition, revealing that the area under these curves increased as a function of information entropy for all E s.

he fitted curves for the direct relationship between information rate and activation in the AIC and ACC were shown in Fig. 4b. he capacity-limited model (logistic function) fitted the relationship between regional activation (i.e., the HRF amplitude) and the information rate better than a simpler linear model for the left AIC ($\Delta BIC = BIC_{linear} - BIC_{logistic} = 11.3$) and the right AIC ($\Delta BIC = 10.0$), indicating that although there was a superadditive activation in these region, the increase of activation was slower in the high information rate conditions compared to the low rate conditions. Moreover, the right AIC revealed a significantly shorter half-time (mean: 7.70) than that of the left AIC (mean ± standard errors: 8.66 ± 0.01; $t_{(26)} = 9.47$, $p < .001$), indicating that the right AIC reached its activation plateau faster. It should be noted that the standard errors (SE) were not reported for the right AIC because the random effects representing the between-subjects difference were not significant. he linear model was preferred for the right ACC ($\Delta BIC = -83.0$), and the fitness of capacity-limited model and of the linear model for the left ACC were not significantly different ($\Delta BIC = 0.9 < 2$), indicating that the activation increased as a linear function of information rate in the left and right ACC. Details of each fitted model are provided in the Supplementary Materials.

he estimates of the CCC were positively correlated to the coefficients of the information entropy × reciprocal of E interaction contrast only in the right AIC (coordinates of the local peak: $x = 30$, $y = 20$, $z = -4$; $= 5.33$, $Z = 4.32$, cluster size $= 105$, corrected cluster level $p = .029$; Fig. 5a), as shown by the whole-brain voxel-wise regression analysis of individual difference in CCC. No significant negative correlation effect was found in any other voxel or region. he patterns of the superadditive activation in the right AIC separated for the median-split of low CCC and high CCC participants are illustrated in Fig. 5b, which shows a greater interaction effect in the right AIC the high CCC participants compared to the low CCC participants. Other properties of the right AIC (i.e., parameter estimates of the capacity-limited model and the grey matter volume) were not significantly correlated to the CCC (see Supplementary Materials for details).

he superadditive activation in the right AIC significantly correlated to individual's FSIQ ($R^2 = 0.37$, $F_{1,\ 25} = 14.89$, $B = 2.71$, $p = .001$). Mediation analysis (Fig. 6) showed that the CCC significantly predicted both superadditive activation in the right AIC (path a, $R^2 = 0.44$, $F_{2,\ 26} = 9.34$, $p = .001$) and FSIQ (path c, $R^2 = 0.30$, $F_{1,\ 25} = 10.73$, $B = 10.45$, $p = .003$). In the regression model with both CCC and the superadditive activation in the right AIC as the predictors of the FSIQ, the coefficient of the superadditive activation in the right AIC (path b) was significant ($B = 1.97$, $p = .023$), while the coefficient of the CCC (path c') was not significant ($B = 5.79 < 10.45$, $p = .110$). hese results indicate that the relationship between the CCC and the FSIQ was fully mediated by the superadditive activation in the right AIC. his mediation effect was not significant for any sub-indices of the IQ (see Supplementary Materials).

3.2. Results of the lesion study

Lesion reconstruction for the AIC group and the ACC group (i.e., patients with unilateral focal lesion in the AIC and ACC, respectively) were shown in Fig. 7a and b. he CCC of the AIC group (3.11 bps; 95% CI: 3.10 to 3.12 bps; range: 2.20 to 3.89 bps; pink bars in Fig. 7c) than significantly lower than in the BDC group (3.98 bps; 95% CI: 3.97 to 4.01 bps; range: 2.71 to 4.83 bps; $p = .018$; the light grey bar in Fig. 7c), and in the NIC group (3.64 bps; 95% CI: 3.63 to 3.65 bps, range: 2.45 to 4.77 bps; $p = .036$; the dark grey bar in Fig. 7c). he difference in CCC between the BDC and NIC groups was not significant ($p = .346$). hese

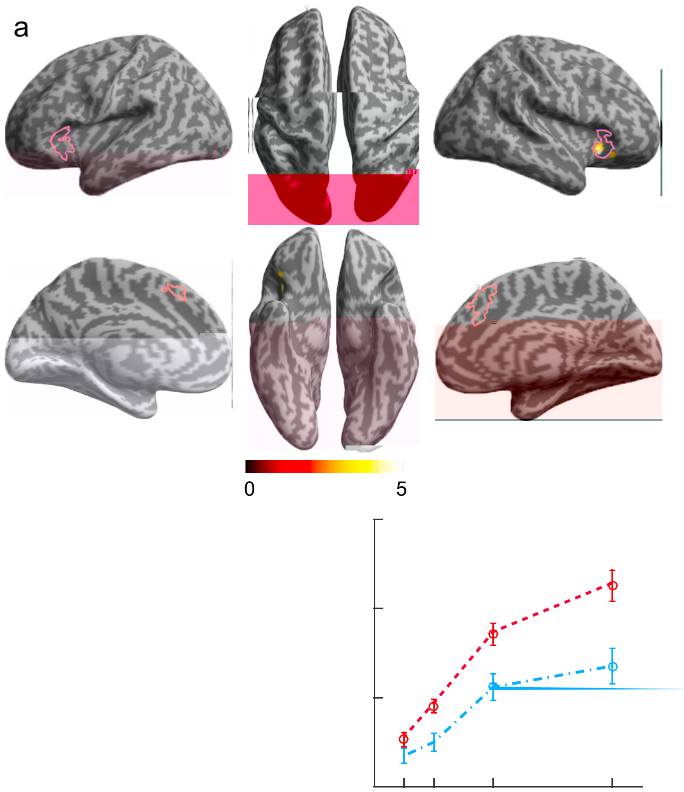

findings indicate a reduction of the CCC in the AIC group, which was not due to the surgery procedure *per se*. In contrast, the CCC of the ACC group (3.72 bps, 95% CI: 3.71 to 3.73 bps, range: 3.34 to 3.93 bps; light pink bars in Fig. 7c) was not significantly different from the BDC group ($p = .405$) and the NIC group ($p = .693$). hese findings indicate that lesions in the ACC were not associated with significant reduction in the CCC. he group-mean accuracy and R in each condition for each group are illustrated in Supplementary Fig. 3.

3.3. Result of network analyses

he connectivity across the regions defined by the conjunction between the main effects of entropy and the reciprocal of E (Fig. 8a) is shown in Fig. 8b (thresholded) and Supplementary Fig. 4 (unthresholded). he estimated community structure of this network revealed four modules: Module 1, including left and right AIC together with the left and right ACC; Module 2, including the left and right FEF together with the left and right IPS; Module 3, including the left and right thalamus together with the left and right caudate nuclei; and Module 4, including the left and right visual areas. his data-driven structure subdivisions were consistent with our definition of the subnetworks of the CCN, with Module 1, 2, and 3 corresponding to the CON, FPN, and subcortical network, respectively.

Across regions of the CCN, the right AIC showed the highest participation coefficient in terms of the inward connections (i.e., connections from other regions to a given region; Supplementary Fig. 5a). Within the CON, the participation coefficient of the right AIC ($63.6 \pm 1.5\%$) was significantly higher than the left AIC ($51.1 \pm 2.3\%$, $t_{26} = 4.61$, $p < .001$) and the left ACC ($59.7 \pm 1.5\%$, $t_{26} = 2.34$, $p = .041$), but not significantly higher than the right ACC ($59.7 \pm 2.0\%$, $t_{26} = 1.92$, $p = .096$; left panel of Fig. 8c). Across regions of the CCN, the left ACC showed the highest participation coefficients in terms of the outward connections (i.e., connections from a given region to other regions; Supplementary Fig. 5b). Within the CON, the participation coefficient of the left ACC ($63.6 \pm 1.5\%$) was significantly higher than the left AIC ($51.1 \pm 2.3\%$, $t_{26} = 4.51$, $p < .001$), the right AIC ($59.7 \pm 1.5\%$, $t_{26} = 3.22$, $p = .006$), and the right ACC ($59.7 \pm 2.0\%$, $t_{26} = 3.59$, $p < .001$; right panel of Fig. 8c). he correlation between participation coefficient of the right AIC and CCC was not significant for the outward connections ($r = -0.01$, $p = .95$) and the inward connections ($r = -0.28$, $p = .15$).

Networks with a simulated unilateral lesion of the AIC and ACC showed decreased global efficiency compared to the non-lesioned network (Fig. 8d and Supplementary able 6). he decrease in global efficiency due to the simulated lesion of the AIC (0.025 ± 0.001) was significantly greater than the decrease due to the simulated lesion of the ACC (0.019 ± 0.001), $F_{1,\ 26} = 16.77$, $p < .001$. he main effect of laterality and the interaction between laterality and brain region were not significant (laterality: $F_{1,\ 26} < 1$; interaction: $F_{1,\ 26} = 2.05$, $p = .164$). Decrease in global efficiency was also found in networks with a simulated lesion of other regions of the CCN (Supplementary Fig. 6). he connections showing significant changes in connectivity after unilateral lesion of the AIC are shown in Supplementary Fig. 7 (also see Supplementary Materials for details).

4. Discussion

4.1. The activation of the AIC is associated with information rate

he superadditive pattern of the AIC activation demonstrates that the AIC is associated with the rate of information processing. In previous studies, we have demonstrated that the activation of regions in the CCN increases as a linear function of information entropy when cognitive control is not overloaded (Fan et al., 2014; Wu et al., 2018). Regional brain response is related to the amount of information being processed (Fan et al., 2014; Harrison et al., 2006; Strange et al., 2005; Wu et al., 2018) and information is encoded by means of neural spikes of defined populations of neurons (Averbeck et al., 2006; Borst and heunissen, 1999). If each bit of information requires a constant number of spikes to be represented, an increase in the amount of the to-be-processed information should be associated with a linear increase of neural activation. If a brain region responds to the rate of information processing, its activation should increase monotonically as a function of information rate, shown as a superadditive effect with both information entropy and E as factors in this study. he main effects and the superadditive activation found in both AIC and ACC indicate that these two regions are the entities responding not only to the information entropy, but also to the rate of information processing under time constrain.

When a region is overloaded by the amount of information to be processed in a given period of time, the resource in terms of neural spikes saturates resulting in information loss (Buschman et al., 2011; Marois and Ivanoff, 2005; Moreno-Bote et al., 2014; Rolls et al., 1997; odd and Marois, 2004; Watanabe and Funahashi, 2014). herefore, the activation plateau of a region indicates that the information to be processed exceeds the maximal amount of information that can be accurately processed in that region in a period of time. Although both AIC and ACC showed a monotonic activation increase as a function of the information rate, only the left and right AIC showed the activation plateau, suggesting that the bilateral AIC, but not the ACC, have a limited resource for cognitive control at least in the range of cognitive load tested in this study. In addition, the right AIC reached its activation plateau earlier than the left AIC, which may suggest that this region is most responsible in limiting the CCC.

he relationship between the cognitive load (measured as information rate in bps) and activation in the AIC and ACC was not confounded by the effect of R on brain activation: the cognitive load, rather than the R , is associated with the amplitude changes of HRF in these regions. An increase in information amount (measured as information entropy in unit of bit) is usually accompanied by prolonged R (Attneave, 1959; Hick, 1952; Hyman, 1953). However, R also depends on processing rate, making it difficult to dissociate the contribution of information entropy and information rate to the R and to the brain activation when only the information entropy is manipulated (Fan et al., 2014; Wu et al., 2018). In this study, we manipulated information entropy via the congruency as well as information rate via the variation of both information entropy and E . We showed that the R decreased and the HRF amplitude in the AIC and ACC increased as a function of E decrease (an increase in information rate) regardless of information entropy. hese results suggest that the information rate is reflected by the HRF amplitude, whereas the information entropy is reflected by the area under the cumulative hemodynamic response curves which can be modeled as the convolution between the HRF with estimated amplitude and the rectangular function with the E as the duration representing the processing time. It is worth noting that these findings were obtained only when response accuracy was emphasized over R . Participants may employ a different mental processing strategy if response speed is emphasized, which may be associated with different brain dynamics.

4.2. The activation of the AIC is associated with the CCC

he bottleneck role of the AIC in cognitive control is further supported by its association with individual differences in terms of CCC. Examining the association between neural responses and task manipulations is a typical approach in cognitive neuroscience to test the involvement of a specifi

the m2in

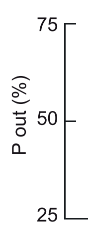

not find a significant deficit in conflict processing i
lesion (Fellows and Farah, 2005; ●u et al., 2012,
2001; Swick and Jovanovic, 2002), suggesting tha
critical region in supporting cognitive control. Si
the CCC in patients with AIC lesions may also sug
in the CCN cannot replace the functional role of the
of the ACC in cognitive control may be compensat
the CCN, such as the AIC and the FEF.

4.4. The AIC as a hub of the CCN

he role of the AIC as a bottleneck of cognitiv
r ed to its role as a hub of the CCN as indic
a he capacity of a high-level cognitive pr
li activity plateau in crucial regions (Ful
al nnectivity among brain regions and

coefficientsimulated AIC and of the CCA AIC significantly impaired the functional integration of the CCN, indicated by reduced network global efficiency. Global efficiency, also called "routing efficiency", reflects the

Corbetta, M., 1998. Frontoparietal cortical networks for directing attention and the eye to visual locations: identical, independent, or overlapping neural systems? PNAS 95, 831–838.

Craig, A.D., 2009. How do you feel—now? the anterior insula and human awareness. Nat. Rev. Neurosci. 10.

Craig, A.D., 2011. Significance of the insula for the evolution of human awareness of feelings from the body. Ann. N. Y. Acad. Sci. 1225, 72–82.

Critchley, H.D., Wiens, S., Rotshtein, P., Dolan, R.J., 2004. Neural systems supporting interoceptive awareness. Nat. Neurosci. 7, 189.

De Baar, H., 1994. von Liebig's law of the minimum and plankton ecology (1899–1991). Prog. Oceanogr. 33, 347–386.

Dosenbach, N.U., Fair, D.A., Cohen, A.L., Schlaggar, B.L., Petersen, S.E., 2008. A dual-networks architecture of top-down control. Trends Cognit. Sci. 12, 99–105.

Dosenbach, N.U., Fair, D.A., Miezin, F.M., Cohen, A.L., Wenger, K.K., Dosenbach, R.A., Fox, M.D., Snyder, A.Z., Vincent, J.L., Raichle, M.E., 2007. Distinct brain networks for adaptive and stable task control in humans. Proc. Natl. Acad. Sci. U. S. A. 104, 11073–11078.

Dosenbach, N.U., Visscher, K.M., Palmer, E.D., Miezin, F.M., Wenger, K.K., Kang, H.C., Burgund, E.D., Grimes, A.L., Schlaggar, B.L., Petersen, S.E., 2006. A core system for the implementation of task sets. Neuron 50, 799–812.

Eckert, M.A., Menon, V., Walczak, A., Ahlstrom, J., Denslow, S., Horwitz, A., Dubno, J.R., 2009. At the heart of the ventral attention system: the right anterior insula. Hum. Brain Mapp. 30, 2530–2541.

Eriksen, B.A., Eriksen, C.W., 1974. Effects of noise letters upon the identification of a target letter in a nonsearch task. Percept. Psychophys. 16, 143–149.

Fan, J., 2014. An information theory account of cognitive control. Front. Hum. Neurosci. 8, 680.

Fan, J., Guise, K.G., Liu, X., Wang, H., 2008. Searching for the majority: algorithms of voluntary control. PLoS One 3, e3522.

Fan, J., Van Dam, N.T., Gu, X., Liu, X., Wang, H., Tang, C.Y., Hof, P.R., 2014. Quantitative characterization of functional anatomical contributions to cognitive control under uncertainty. J. Cogn. Neurosci. 26, 1490–1506.

Fellows, L.K., Farah, M.J., 2005. Is anterior cingulate cortex necessary for cognitive control? Brain 128, 788–796.

Flynn, F.G., 1999. Anatomy of the insula functional and clinical correlates. Aphasiology 13, 55–78.

Friedman, N., Goldszmidt, M., Wyner, A., 1999. Data analysis with Bayesian networks: a bootstrap approach. In: Proceedings of the Fifteenth Conference on Uncertainty in Artificial Intelligence. Morgan Kaufmann Publishers Inc., pp. 196–205

Friston, K.J., Fletcher, P., Josephs, O., Holmes, A., Rugg, M., Turner, R., 1998. Event-related fMRI: characterizing differential responses. Neuroimage 7, 30–40.

Friston, K.J., Holmes, A.P., Worsley, K.J., Poline, J.P., Frith, C.D., Frackowiak, R.S., 1994. Statistical parametric maps in functional imaging: a general linear approach. Hum. Brain Mapp. 2, 189–210.

Friston, K.J., Li, B., Daunizeau, J., Stephan, K.E., 2011. Network discovery with DCM. Neuroimage 56, 1202–1221.

Fukuda, K., Awh, E., Vogel, E.K., 2010. Discrete capacity limits in visual working memory. Curr. Opin. Neurobiol. 20, 177–182.

Gorban, A.N., Pokidysheva, L.I., Smirnova, E.V., Tyukina, T.A., 2011. Law of the minimum paradoxes. Bull. Math. Biol. 73, 2013–2044.

Gratton, C., Sun, H., Petersen, S.E., 2017. Control networks and hubs. Psychophysiology 55 (3), e13032.

Gu, X., Gao, Z., Wang, X., Liu, X., Knight, R.T., Hof, P.R., Fan, J., 2012. Anterior insular cortex is necessary for empathetic pain perception. Brain 135, 2726–2735.

Gu, X., Hof, P.R., Friston, K.J., Fan, J., 2013. Anterior insular cortex and emotional awareness. J. Comp. Neurol. 521, 3371–3388.

Gulbinaite, R., van Rijn, H., Cohen, M.X., 2014. Fronto-parietal network oscillations reveal relationship between working memory capacity and cognitive control. Front. Hum. Neurosci. 8, 761.

Harrison, L.M., Duggins, A., Friston, K.J., 2006. Encoding uncertainty in the hippocampus. Neural Network. 19, 535–546.

Hasson, U., Avidan, G., Deouell, L.Y., Bentin, S., Malach, R., 2003. Face-selective activation in a congenital prosopagnosic subject. J. Cogn. Neurosci. 15, 419–431.

Hick, W.E., 1952. On the rate of gain of information. Q. J. Exp. Psychol. 4, 11–26.

Hu, S., Ide, J.S., Zhang, S., Li, C.S.R., 2015. Anticipating conflict: neural correlates of a Bayesian belief and its motor consequence. Neuroimage 119, 286–295.

Hyman, R., 1953. Stimulus information as a determinant of reaction time. J. Exp. Psychol. 45, 188.

Jeong, H., Tombor, B., Albert, R., Oltvai, Z.N., Barabási, A.-L., 2000. The Large-Scale Organization of Metabolic Networks. Nature 407, 651–654. https://www.nature.com/articles/35036627.

Kelly, C., Toro, R., Di Martino, A., Cox, C.L., Bellec, P., Castellanos, F.X., Milham, M.P., 2012. A convergent functional architecture of the insula emerges across imaging modalities. Neuroimage 61, 1129–1142.

Kinnison, J., Padmala, S., Choi, J.-M., Pessoa, L., 2012. Network analysis reveals increased integration during emotional and motivational processing. J. Neurosci. 32, 8361–8372.

Koziol, L.F., 2014. Cognitive Control, Reward, and the Basal Ganglia. The Myth of Executive Functioning. Springer, pp. 61–64.

Mackie, M.-A., Van Dam, N.T., Fan, J., 2013. Cognitive control and attentional functions. Brain Cogn. 82, 301–312.

Marois, R., Ivanoff, J., 2005. Capacity limits of information processing in the brain. Trends Cognit. Sci. 9, 296–305.

Mazziotta, J.C., Toga, A.W., Evans, A., Fox, P., Lancaster, J., 1995. A probabilistic atlas of the human brain: theory and rationale for its development. Neuroimage 2, 89–101.

Medford, N., Critchley, H.D., 2010. Conjoint activity of anterior insular and anterior cingulate cortex: awareness and response. Brain Struct. Funct. 214, 535–549.

Menon, V., Uddin, L.Q., 2010. Saliency, switching, attention and control: a network model of insula function. Brain Struct. Funct. 214, 655–667.

Misic, B., Sporns, O., McIntosh, A.R., 2014. Communication efficiency and congestion of signal traffic in large-scale brain networks. PLoS Comput. Biol. 10, e1003427.

Mooney, C.Z., Duval, R.D., 1993. Bootstrapping: A Nonparametric Approach to Statistical Inference (No. 95). Sage.

Moreno-Bote, R., Beck, J., Kanitscheider, I., Pitkow, X., Latham, P., Pouget, A., 2014. Information-limiting correlations. Nat. Neurosci. 17, 1410–1417.

Nelson, S.M., Dosenbach, N.U., Cohen, A.L., Wheeler, M.E., Schlaggar, B.L., Petersen, S.E., 2010. Role of the anterior insula in task-level control and focal attention. Brain Struct. Funct. 214, 669–680.

Neubauer, A.C., Fink, A., 2009. Intelligence and neural efficiency. Neurosci. Biobehav. Rev. 33, 1004–1023.

Newman, M., 2010. Networks: an Introduction. Oxford University Press.

Niendam, T.A., Laird, A.R., Ray, K.L., Dean, Y.M., Glahn, D.C., Carter, C.S., 2012. Meta-analytic evidence for a superordinate cognitive control network subserving diverse executive functions. Cognit. Affect Behav. Neurosci. 12, 241–268.

Ochsner, K.N., Kosslyn, S.M., Cosgrove, G.R., Cassem, E.H., Price, B.H., Nierenberg, A.A., Rauch, S.L., 2001. Deficits in visual cognition and attention following bilateral anterior cingulotomy. Neuropsychologia 39, 219–230.

Palva, J.M., Monto, S., Kulashekhar, S., Palva, S., 2010. Neuronal synchrony reveals working memory networks and predicts individual memory capacity. Proc. Natl. Acad. Sci. U. S. A. 107, 7580–7585.

Posner, M.I., Snyder, C., 1975. Attention and Cognitive Control. Information Processing and Cognition: the Loyola Symposium. Erlbaum, Hillsdale NJ, pp. 55–85.

Power, J.D., Schlaggar, B.L., Lessov-Schlaggar, C.N., Petersen, S.E., 2013. Evidence for hubs in human functional brain networks. Neuron 79, 798–813.

Raichle, M.E., MacLeod, A.M., Snyder, A.Z., Powers, W.J., Gusnard, D.A., Shulman, G.L., 2001. A default mode of brain function. Proc. Natl. Acad. Sci. U. S. A. 98, 676–682.

Rissman, J., Gazzaley, A., D'Esposito, M., 2004. Measuring functional connectivity during distinct stages of a cognitive task. Neuroimage 23, 752–763.

Rolls, E.T., Treves, A., Tovee, M.J., 1997. The representational capacity of the distributed encoding of information provided by populations of neurons in primate temporal visual cortex. Exp. Brain Res. 114, 149–162.

Rossi, A.F., Pessoa, L., Desimone, R., Ungerleider, L.G., 2009. The prefrontal cortex and the executive control of attention. Exp. Brain Res. 192, 489–497.

Rubinov, M., Sporns, O., 2010. Complex network measures of brain connectivity: uses and interpretations. Neuroimage 52, 1059–1069.

Sattler, J.M., Ryan, J.J., 2009. Assessment with the WAIS-IV. Jerome M Sattler Publisher.

Schwab, J., Bialow, M., Clemmons, R., Martin, P., Holzer, C., 1967. The Beck depression inventory with medical inpatients. Acta Psychiatr. Scand. 43, 255–266.

Schwarz, G., 1978. Estimating the dimension of a model. Ann. Stat. 6, 461–464.

Scutari, M., Nagarajan, R., 2011. On identifying significant edges in graphical models. In: Proceedings of Workshop on Probabilistic Problem Solving in Biomedicine. Springer-Verlag, Bled, Slovenia, pp. 15–27.

Shannon, C.E., Weaver, W., 1949. The Mathematical Theory of Communication, vol. 5. University of Illinois Press, Urbana.

Singer, T., Critchley, H.D., Preuschoff, K., 2009. A common role of insula in feelings, empathy and uncertainty. Trends Cognit. Sci. 13, 334–340.

Spagna, A., Dufford, A.J., Wu, Q., Wu, T., Zheng, W., Coons, E.E., Hof, P.R., Hu, B., Wu, Y., Fan, J., 2018a. Gray matter volume of the anterior insular cortex and social networking. J. Comp. Neurol. 526, 1183–1194.

Spagna, A., He, G., Jin, S., Gao, L., Mackie, M.-A., Tian, Y., Wang, K., Fan, J., 2018b. Deficit of supramodal executive control of attention in schizophrenia. J. Psychiatr. Res. 97, 22–29.

Spagna, A., Mackie, M.-A., Fan, J., 2015. Supramodal executive control of attention. Front. Psychol. 6, 65.

Sporns, O., 2013. Network attributes for segregation and integration in the human brain. Curr. Opin. Neurobiol. 23, 162–171.

Sridharan, D., Levitin, D.J., Menon, V., 2008. A critical role for the right fronto-insular cortex in switching between central-executive and default-mode networks. Proc. Natl. Acad. Sci. U. S. A. 105, 12569–12574.

Strange, B.A., Duggins, A., Penny, W., Dolan, R.J., Friston, K.J., 2005. Information theory, novelty and hippocampal responses: unpredicted or unpredictable? Neural Network. 18, 225–230.

Stroop, J.R., 1935. Studies of interference in serial verbal reactions. J. Exp. Psychol. 18, 643.

Swick, D., Jovanovic, J., 2002. Anterior cingulate cortex and the Stroop task: neuropsychological evidence for topographic specificity. Neuropsychologia 40, 1240–1253.

Tellegen, A., Briggs, P.F., 1967. Old wine in new skins: grouping Wechsler subtests into new scales. J. Consult. Psychol. 31, 499.

Todd, J.J., Marois, R., 2004. Capacity limit of visual short-term memory in human posterior parietal cortex. Nature 428, 751–754.

Tombu, M.N., Asplund, C.L., Dux, P.E., Godwin, D., Martin, J.W., Marois, R., 2011. A unified attentional bottleneck in the human brain. Proc. Natl. Acad. Sci. Unit. States Am. 108, 13426–13431.

Tsamardinos, I., Brown, L.E., Aliferis, C.F., 2006. The max-min hill-climbing Bayesian network structure learning algorithm. Mach. Learn. 65, 31–78.

van den Heuvel, M.P., Kahn, R.S., Goñi, J., Sporns, O., 2012. High-cost, high-capacity backbone for global brain communication. Proc. Natl. Acad. Sci. Unit. States Am. 109, 11372–11377.

van den Heuvel, M.P., Sporns, O., 2011. Rich-club organization of the human connectome. J. Neurosci. 31, 15775–15786.

van den Heuvel, M.P., Sporns, O., 2013. Network hubs in the human brain. rends Cognit. Sci. 17, 683–696.

Vogel, E.K., Awh, E., 2008. How to exploit diversity for scientific gain: using individual differences to constrain cognitive theory. Curr. Dir. Psychol. Sci. 17, 171–176.

Wang, H., Liu, X., Fan, J., 2011. Cognitive control in majority search: a computational modeling approach. Front. Hum. Neurosci. 5, 16.

Watanabe, K., Funahashi, S., 2014. Neural mechanisms of dual-task interference and cognitive capacity limitation in the prefrontal cortex. Nat. Neurosci. 17, 601–611.

Wu, ., Dufford, A.J., Egan, L.J., Mackie, M.-A., Chen, C., Yuan, C., Chen, C., Li, X., Liu, X., Hof, P.R., 2018. Hick–yman law is mediated by the cognitive control network in the brain. Cerebr. Cortex 28, 2267–2282.

Wu, ., Dufford, A.J., Mackie, M.-A., Egan, L.J., Fan, J., 2016. he capacity of cognitive control estimated from a perceptual decision making task. Sci. Rep. 6, 34025.